PNAS RESEARCH ARTICLE | MICROBIOLOGY

Spatial heterogeneity in biofilm metabolism elicited by local control of phenazine methylation

Christopher R. Evans[a,1], Marina K. Smiley[a,1], Sean Asahara Thio[a], Mian Wei[b], Lindsey C. Florek[a], Hannah Dayton[a], Alexa Price-Whelan[a], Wei Min[b], and Lars E. P. Dietrich[a,2]

Edited by Caroline Harwood, University of Washington, Seattle, WA; received August 2, 2023; accepted September 15, 2023

Within biofilms, gradients of electron acceptors such as oxygen stimulate the formation of physiological subpopulations. This heterogeneity can enable cross-feeding and promote drug resilience, features of the multicellular lifestyle that make biofilm-based infections difficult to treat. The pathogenic bacterium *Pseudomonas aeruginosa* produces pigments called phenazines that can support metabolic activity in hypoxic/anoxic biofilm subzones, but these compounds also include methylated derivatives that are toxic to their producer under some conditions. In this study, we uncover roles for the global regulators RpoS and Hfq/Crc in controlling the beneficial and detrimental effects of methylated phenazines in biofilms. Our results indicate that RpoS controls phenazine methylation by modulating activity of the carbon catabolite repression pathway, in which the Hfq/Crc complex inhibits translation of the phenazine methyltransferase PhzM. We find that RpoS indirectly inhibits expression of CrcZ, a small RNA that binds to and sequesters Hfq/Crc, specifically in the oxic subzone of *P. aeruginosa* biofilms. Deletion of *rpoS* or *crc* therefore leads to overproduction of methylated phenazines, which we show leads to increased metabolic activity—an apparent beneficial effect—in hypoxic/anoxic subpopulations within biofilms. However, we also find that under specific conditions, biofilms lacking RpoS and/or Crc show increased sensitivity to phenazines indicating that the increased metabolic activity in these mutants comes at a cost. Together, these results suggest that complex regulation of PhzM allows *P. aeruginosa* to simultaneously exploit the benefits and limit the toxic effects of methylated phenazines.

biofilm physiology | pyocyanin | carbon catabolite repression | metabolic heterogeneity | self-resistance

Significance

Pseudomonas aeruginosa causes biofilm-based infections and is known for its production of colorful phenazine derivatives. Among these, the methylated phenazines are the most toxic and can cause condition-dependent damage to their producer. Here, we show that the methylated phenazine pyocyanin also has a beneficial effect in that it supports metabolic activity at depth in biofilms, where oxygen limitation would otherwise stall metabolism. We describe a link between *P. aeruginosa* global regulators, which control methylated phenazine production in a manner that limits the toxicity of these compounds while simultaneously enabling their contribution to metabolism. These results expand our understanding of the strategies that enable *P. aeruginosa* survival in multicellular structures, which is key to its success during chronic host colonization.

Cellular growth at high density promotes the formation of resource gradients, and multicellular structures therefore contain microenvironments with distinct conditions. To maintain metabolic activity, cells within multicellular structures undergo physiological differentiation, which enhances robustness of the overall population (1–5). Coexistence in a multicellular structure also allows differentiated subpopulations to interact in beneficial ways, for example, by exchanging metabolites that are optimally produced in one region and consumed in another. The physiological heterogeneity of multicellular structures is problematic in infections or cancers, where the effectiveness of a drug often depends on the metabolic status of target cells (6). Approaches that provide insight into physiological differentiation while retaining information about structure can help us to understand the unique biology of multicellularity and can also inform treatment methods.

Microbial biofilms are multicellular structures that exhibit metabolic differentiation and developmental responses to resource limitation, with parallels in metazoans and plants (2, 7). Studies in diverse bacteria have indicated that sigma factors, which are regulatory proteins that mediate transcriptional responses to environmental and physiological cues, are key players in biofilm biology (8–13). The sigma factor is a component of the RNA polymerase that confers specificity for target sequences in promoters, and bacterial genomes typically encode more than one sigma factor with different specificities (8, 14). Thus, condition-dependent shifts in the sigma factor pool allow bacteria to elicit global changes in their transcriptional profiles, which adapt their physiology to their current environment. One of the best-studied sigma factors is RpoS, which is conserved in proteobacteria and typically activates gene expression in the stationary phase of planktonic growth or during resource limitation (15–18).

The bacterium *Pseudomonas aeruginosa* is a prevalent cause of biofilm-based infections and a model for the study of biofilm development and metabolism. It can adapt to environmental changes over the long term, with its high mutation rate (19–22), and in the short term, with an arsenal of up to 26 sigma factors (depending on strain identity) and hundreds of transcription factors (23–25). These regulators form a complex network of gene expression control that we are only beginning to understand holistically (24, 25).

Author contributions: C.R.E., M.K.S., M.W., A.P.-W., and L.E.P.D. designed research; C.R.E., M.K.S., S.A.T., M.W., L.C.F., and H.D. performed research; W.M. contributed new reagents/analytic tools; C.R.E., M.K.S., S.A.T., M.W., L.C.F., H.D., A.P.-W., and L.E.P.D. analyzed data; and C.R.E., M.K.S., A.P.-W., and L.E.P.D. wrote the paper.

The authors declare no competing interest.

This article is a PNAS Direct Submission.

[1]C.R.E. and M.K.S. contributed equally to this work.

[2]To whom correspondence may be addressed. Email: LDietrich@columbia.edu.

This article contains supporting information online at https://www.pnas.org/lookup/suppl/doi:10.1073/pnas.2313208120/-/DCSupplemental.

Published October 17, 2023.

Our knowledge about the roles of sigma factor-controlled networks in regulating gene expression and affecting *P. aeruginosa* physiology is particularly limited for cells surviving in more complex environments like biofilms.

RpoS is required for wild-type *P. aeruginosa* biofilm development in a variety of assays and across strain backgrounds. It is expressed in biofilms, particularly at the biofilm–air interface, in *Escherichia coli* and *P. aeruginosa* and its regulon includes genes involved in crucial redox metabolism in the oxic biofilm subzone (10, 26–28). Furthermore, *rpoS* mutants have been reported to overproduce pyocyanin (1-hydroxy-5-methylphenazine) (29), one of several phenazine compounds that allow *P. aeruginosa* to carry out extracellular electron transfer when respiratory electron acceptors are limiting (such as within biofilms) (30–32). While studies in biofilms have indicated that this electron-shuttling property of phenazines supports metabolic activity, recent work has also shown that phenazines can be toxic to *P. aeruginosa* under specific conditions or when their production and localization are not properly controlled (33–35).

In this study, we examined the role of RpoS in *P. aeruginosa* PA14 biofilm physiology and were intrigued to find that this sigma factor has an inhibitory effect on metabolic activity at depth in biofilms. At first glance, an inhibition of metabolic activity seems detrimental, and we sought to understand how and why a major regulator would mediate this effect. Here, we describe the identification of a regulatory pathway and of phenazine products that act downstream of RpoS to modulate metabolic activity. Our findings implicate this pathway in methylated phenazine resistance and suggest that modulation of phenazine methylation is critical for balancing the toxic and beneficial effects of these reactive compounds in *P. aeruginosa* biofilms.

Results

RpoS Attenuates Biofilm Metabolic Activity. Prior work has indicated that RpoS is active in biofilms and that it confers fitness during conditions of either carbon source or oxygen limitation in *P. aeruginosa* (36, 37). We therefore sought to test whether RpoS contributes to metabolic activity in macrocolony biofilms, which contain opposing oxygen and carbon-source gradients (38, 39). Our group has previously used stimulated Raman scattering (SRS) microscopy to map metabolic activity across biofilm depth and found that it is affected by growth conditions and genotype (31, 39). SRS microscopy is an optical imaging technique that detects the vibration of specific chemical bonds (40). For this method, we transfer mature biofilms onto medium containing deuterated water for 5 h before harvesting and preparing thin sections and then use SRS to detect the D-C bonds that arise from incorporation of deuterium into biomass (an indicator of metabolic activity) (Fig. 1*A*). We used this approach and observed two changes in Δ*rpoS* biofilms when compared to WT: i) a shift in the localization of maximum metabolic activity, from a depth of ~50 to 30 μm, and ii) an overall increase in metabolic activity over a broad region starting at a depth of about 50 μm and continuing toward the biofilm base (Fig. 1*B*).

The Methylated Phenazine Pyocyanin Supports Metabolic Activity across Depth in PA14 Biofilms. We have previously reported that phenazine production (Fig. 2*A*) enhances metabolic activity at depth in PA14 biofilms (31), and we therefore hypothesized that the effects of RpoS on biofilm metabolic activity could be mediated by effects on phenazine production. To test this, we used SRS microscopy to image biofilm thin sections from a Δ*rpoS*Δ*phz* mutant, which is unable to produce phenazines. Removing the capacity to produce phenazines abolished the enhanced metabolic activity of the Δ*rpoS* parent strain, indicating that this phenotype is indeed phenazine-dependent (Fig. 2*B*). We note that the absence of phenazines did not affect the depth at which the maximum metabolic activity was detected in Δ*rpoS* biofilms. The localization of maximum metabolic activity may be affected by differences in oxygen consumption in Δ*rpoS* biofilms as we observed steeper oxygen gradients in this mutant background when compared to respective parent-strain backgrounds (Fig. 2*C*).

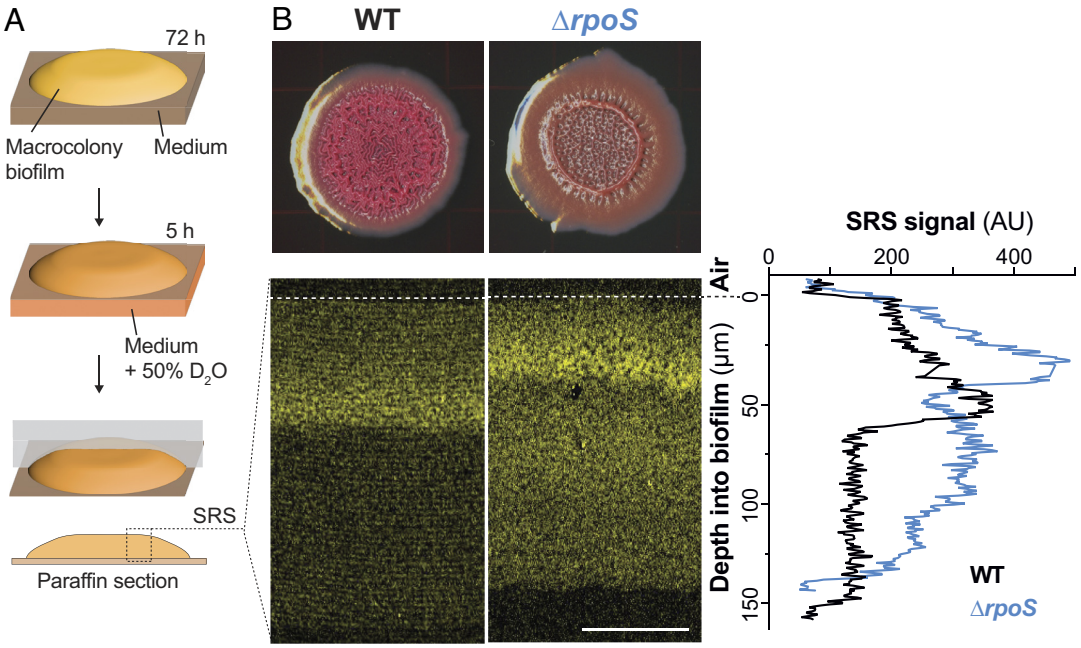

Fig. 1. Δ*rpoS* biofilms show increased metabolic activity at depth when compared to those formed by WT PA14. (*A*) Scheme depicting the preparation of macrocolony biofilm thin sections for imaging by stimulated Raman scattering (SRS) microscopy. (*B*) *Top*: PA14 and Δ*rpoS* biofilms grown for 72 h on 1% tryptone, 1% agar medium containing the dyes Congo red and Coomassie blue. *Bottom*: SRS microscopy images of PA14 and Δ*rpoS* biofilm thin sections. The air interface of each biofilm is indicated by a dotted line. The SRS signal is indicative of metabolic activity and is false-colored yellow. Right: quantification of average SRS signal across depth. Experiments were performed in biological triplicate and representative images are shown (Scale bar, 50 μm).

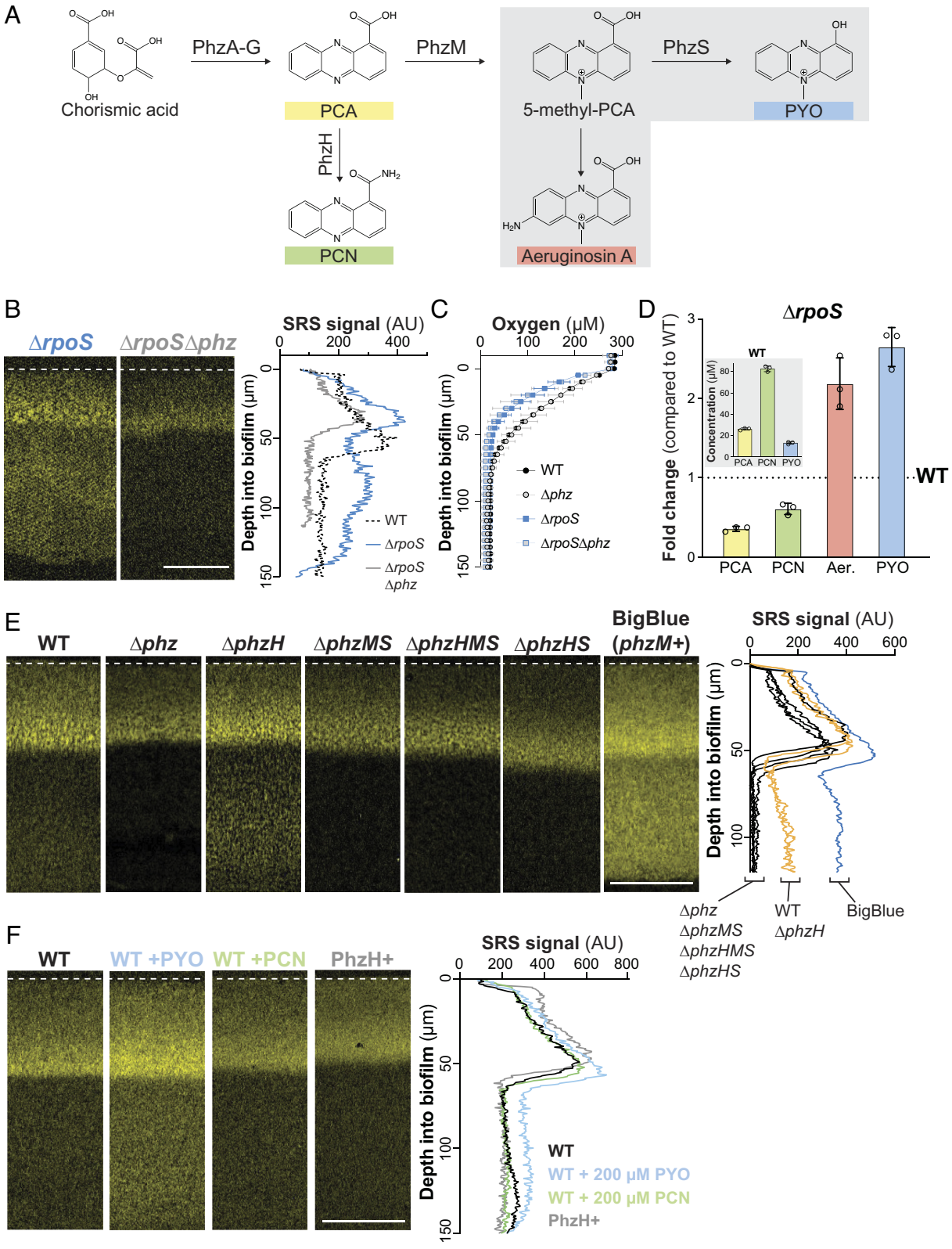

Fig. 2. Biofilm metabolic activity at depth is supported specifically by the production of methylated phenazine derivatives. (*A*) The phenazine biosynthetic pathway. A series of enzymes convert two molecules of chorismate to phenazine-1-carboxylic acid (PCA). PCA can be aminated by PhzH to produce phenazine-1-carboxamide (PCN) or methylated by PhzM to produce 5-methyl-PCA. Further modification of 5-methyl-PCA abiotically by free amine groups or enzymatically by PhzS produces aeruginosins (one example structure is shown) or pyocyanin (PYO), respectively. (*B*) SRS microscopy images of thin sections prepared from Δ*rpoS* and Δ*rpoS*Δ*phz* macrocolony biofilms. (*C*) Change in oxygen concentration along the depth of biofilms. Data shown are the mean of biological triplicates and error bars represent SD. (*D*) Change in phenazine production by Δ*rpoS* biofilms relative to biofilms formed by WT PA14. *Inset*: absolute concentrations of phenazines from WT colonies. Biofilms were grown on 1% tryptone, 1% agar for 72 h. Aer., aeruginosins. Individual points represent biological replicates and error bars represent SD. (*E*) SRS microscopy images of thin sections prepared from PA14 WT and phenazine biosynthetic mutant biofilms. (*F*) SRS microscopy images of WT and PhzH+ (containing an extra copy of *phzH* under the control of a constitutive promoter) biofilm thin sections. Where indicated, WT biofilms were exposed to 0.2 M of the specified phenazines for 5 h. For (*B*, *E*, and *F*), SRS signal is false-colored yellow; quantification of the average SRS signal across depth is shown in the right-hand panels, and experiments were performed in biological triplicate and representative images are shown (Scale bars, 50 μm).

Due to the importance of phenazines in the high metabolic activity of Δ*rpoS* biofilms, we investigated how RpoS affects the production of specific phenazine derivatives. *P. aeruginosa* phenazines are produced in biofilms and in the stationary phase during growth in shaken liquid cultures (41). The first derivative produced in the *P. aeruginosa* phenazine synthesis pathway is phenazine-1-carboxylic acid (PCA), which can be converted to i) phenazine-1-carboxamide (PCN) via the PhzH transamidase, or ii) 5-methyl-PCA via the PhzM methyltransferase. 5-methyl-PCA, an unstable intermediate, is converted to other methylated phenazines including pyocyanin and aeruginosin A (42–44) (Fig. 2*A*). It has been reported that RpoS inhibits production of PhzM and that RpoS-deficient mutants show increased pyocyanin and decreased PCA production (29, 45). HPLC and spectrophotometer analysis of extracts from biofilms and the underlying growth medium confirmed that flux through the PhzM step of the phenazine biosynthetic pathway was increased in Δ*rpoS* biofilms (Fig. 2*D*). Furthermore, PCA levels in PA14 and Δ*rpoS* biofilms lacking the phenazine modification enzymes PhzH, PhzM, and PhzS (Δ*phzHMS*) were similar, providing further evidence that the changes in phenazine differentiation observed in Δ*rpoS* biofilms is due to changes in regulation of one or more enzyme(s) that modify PCA (*SI Appendix*, Fig. S1*A*).

To evaluate whether specific phenazine derivatives contribute to metabolic activity in biofilms and whether this underpins the Δ*rpoS* phenotype, we incubated mutant biofilms lacking genes for phenazine-modification enzymes on deuterated water, prepared thin sections, and imaged via SRS microscopy. We observed a clear correlation between the production of pyocyanin and the amount of metabolic activity across depth in biofilms, most notably in the hypoxic/anoxic zone. Consistent with the notion that one or more methylated phenazines promote metabolic activity, a strain ("BigBlue") that contains a second copy of *phzM* on the chromosome (46) and therefore overproduces methylated phenazines (*SI Appendix*, Fig. S1*B*), showed the strongest SRS signal (Fig. 2*E*). Among the mutants we tested was Δ*phzHS*, which would be expected to produce increased levels of 5-methyl-PCA, aeruginosin A, and other abiotic 5-methyl-PCA derivatives (relative to WT) without producing pyocyanin. Interestingly, Δ*phzHS* biofilms exhibited an SRS profile that resembled that of Δ*phzHMS* biofilms, showing that specific disruption of pyocyanin synthesis abolishes metabolic activity in the biofilm anoxic zone. By adding endogenous pyocyanin to mature biofilms, we also found that this methylated phenazine is sufficient to promote metabolic activity at depth (Fig. 2*F*). In addition, since PCN is the most abundant phenazine in macrocolony biofilms (Fig. 2*D*) (41), we tested the effect of this compound on metabolic activity. In contrast to our observations for pyocyanin, our results for engineered strains with altered PCN production and for biofilms exposed to PCN indicated that this phenazine does not contribute to metabolic activity at depth in biofilms (Fig. 2 *E* and *F*).

RpoS Regulates Phenazine Derivatization Via the *P. aeruginosa* Carbon Catabolite Repression System. We sought to further understand the regulatory pathway that allows RpoS to control phenazine methylation. The *phzM* transcript is one of >200 mRNA targets of the Hfq/Crc ("catabolite repression control") protein complex (Fig. 3*A*) (47–50). The Hfq/Crc complex mediates the terminal regulatory step of the carbon catabolite repression (CCR) pathway. Canonically, the CCR pathway acts to inhibit translation of mRNAs that support the use of nonpreferred carbon sources when preferred substrates are available (51, 52), though recent studies have indicated that it has broad effects on *P. aeruginosa* physiology beyond primary metabolic functions (53–55). Consistent with the notion that RpoS acts via this pathway to control phenazine methylation, a recent study (45) found that the translation of *phzM* is inhibited by RpoS. To further probe this model, we created Δ*crc* and Δ*rpoS*Δ*crc* mutants and measured phenazine production by biofilms. We found that like Δ*rpoS* biofilms, Δ*crc* and Δ*rpoS*Δ*crc* biofilms show enhanced production of methylated phenazines (Fig. 3*B*). Δ*crc* biofilms differ from Δ*rpoS* biofilms in that they do not show a substantial decrease in PCA and PCN production compared to WT. This indicates that although both Hfq/Crc and RpoS have global regulatory effects (18, 50), the impact of Crc on nonmethylated phenazines is negligible or small compared to that of RpoS. RpoS affects the expression of over 700 genes (18), one or more of which likely has downstream effects on the production of the nonmethylated phenazines.

RpoS Inhibits *crcZ* Expression. Binding of the Hfq/Crc complex to target transcripts can be prevented by the small RNA CrcZ (Fig. 3*A*), which itself can bind and thereby sequester Hfq/Crc under appropriate conditions. This regulatory mechanism allows for condition-dependent translation of Hfq/Crc targets (52). RpoS could therefore affect Hfq/Crc activity by modulating transcription of either *crcZ* or *crc*. To test this, we created constructs in which the upstream promoter regions of *crcZ* or *crc* are cloned in front of *mScarlet* (P*crcZ* and P*crc*, respectively) and then placed these in a neutral site on the chromosome in WT and Δ*rpoS* backgrounds. We found that in both biofilms and liquid (planktonic) cultures, removal of RpoS did not affect activity of P*crc*, but, in contrast, led to a strong enhancement of P*crcZ* activity (Fig. 3*C* and *SI Appendix*, Fig. S2*A*). This indicates that RpoS inhibits *crcZ* expression, possibly by competing with RpoN for RNA polymerase (56) (Fig. 3*A*) or another more indirect mechanism.

The resource gradients that form across depth in macrocolony biofilms lead to physiological differentiation and subpopulations with distinct patterns of gene expression (2, 4, 5, 26, 57). RpoS-dependent effects on gene expression could be localized to a specific biofilm subzone, perhaps where this activity would be most physiologically relevant. Indeed, results from previous studies suggest that RpoS is most expressed and active at the *P. aeruginosa* biofilm–air interface (26, 27, 58, 59). Moreover, pyocyanin synthesis requires oxygen, and prior work by our group has indicated that production of 5-Me-PCA may also be limited to oxygen-containing biofilm subzones (60). When we prepared thin sections of WT and Δ*rpoS* biofilms expressing P*crcZ-mScarlet* and imaged by fluorescence microscopy, we found that the effect of RpoS on *crcZ* expression was indeed localized to the biofilm-air interface (Fig. 3*D*), similar to what has been observed for direct RpoS targets such as the promoter for *coxB* (26, 38). The observation that RpoS inhibits *crcZ* expression specifically at the biofilm-air interface, which is the biofilm region furthest from the growth medium, is consistent with a role for RpoS and the CCR system in inhibiting methylated phenazine production. Because phenazines are excreted small molecules with the potential to diffuse through the biofilm, changes in phenazine derivatization due to changes in RpoS activity at the biofilm surface can negatively impact metabolic activity at depth in biofilms (Fig. 1*B*).

Evidence suggests that *crcZ* transcription in *P. aeruginosa* is driven directly by the regulator CbrB and the sigma factor RpoN (Fig. 3*A* and *SI Appendix*, Fig. S2 *A* and *B*) (24, 52, 61). CbrB is part of the CbrAB two-component system, which responds to an as-yet-unidentified cue. Our observation that RpoS inhibits *crcZ* transcription raised the question of whether RpoS might be acting upstream of CbrAB. To test this, we deleted *cbrB* in the Δ*rpoS* P*crcZ-mScarlet* reporter strain and found that this abolished P*crcZ* activity (*SI Appendix*, Fig. S2*B*). These results indicate that CbrB is required for *crcZ* repression in the Δ*rpoS* background and are

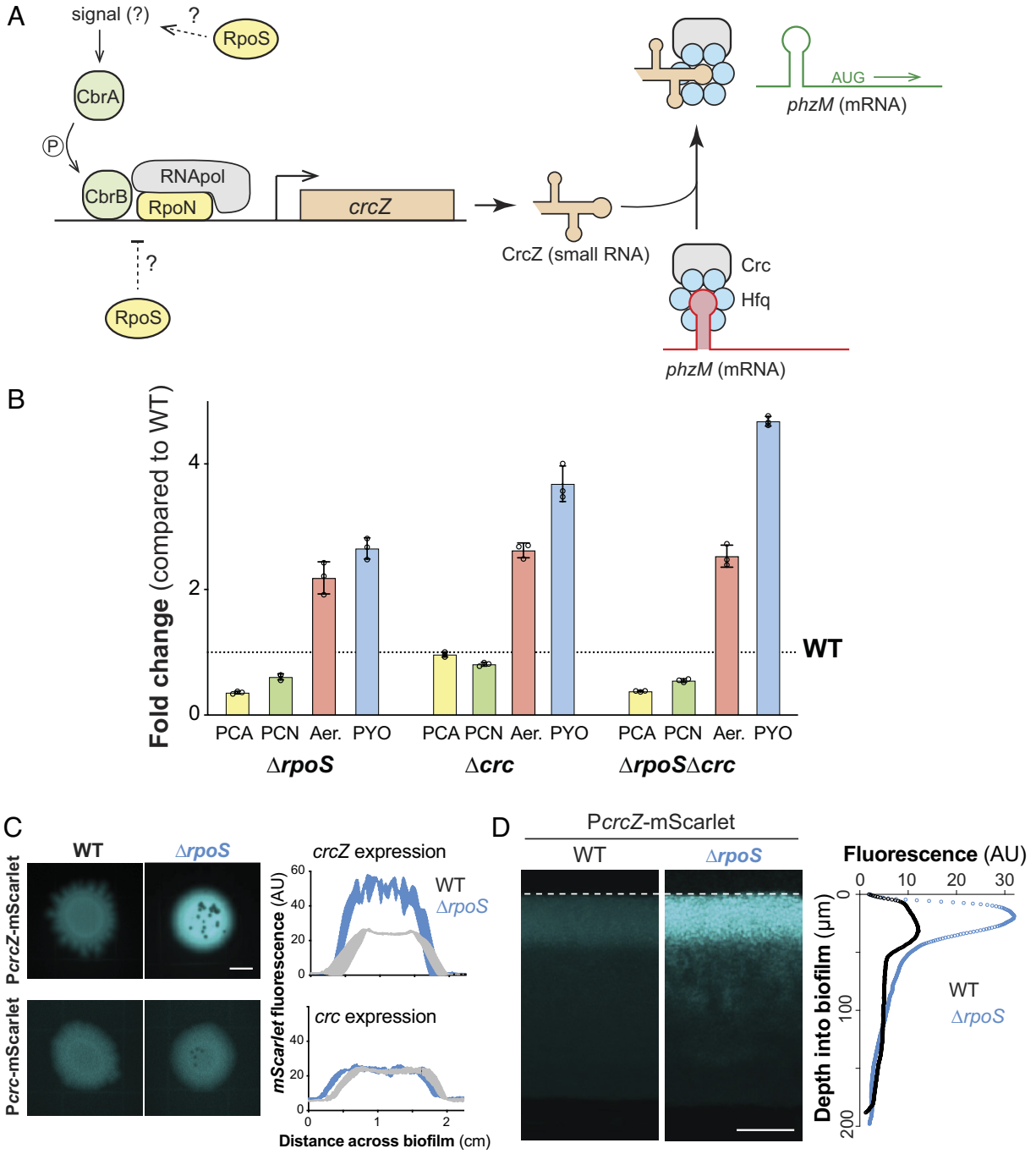

Fig. 3. RpoS inhibits phenazine methylation by modulating the carbon catabolite repression pathway at the biofilm-air interface. (*A*) Schematic of the *P. aeruginosa* carbon catabolite repression pathway, which controls translation of *phzM* in a carbon source-dependent manner. RpoN is the canonical sigma factor that is associated with this pathway and it acts in conjunction with the transcription factor CbrB. When CrcZ levels are low, the Crc/Hfq complex binds to *phzM* transcript and inhibits translation. When CrcZ levels are high, CrcZ binds and sequesters Crc/Hfq, allowing translation of the *phzM* transcript. (*B*) Changes in production of phenazine derivatives by Δ*rpoS*, Δ*crc*, and Δ*rpoS*Δ*crc* biofilms relative to biofilms formed by WT PA14. Individual points represent biological triplicates and error bars represent SD. (*C*) Representative whole-biofilm fluorescence images of PA14 WT and Δ*rpoS* strains expressing mScarlet under control of P*crcZ* or P*crc* (Scale bar, 5 mm). mScarlet fluorescence is false-colored cyan. The average levels of fluorescence produced by each strain along the diameter of three independent, biological-replicate biofilms with the P*crc-mScarlet* or P*crcZ-mScarlet* reporters are shown in the right-hand plots. Shading indicates the SD. (*D*) Fluorescence microscopy of thin sections prepared from WT PA14 and Δ*rpoS* biofilms expressing P*crcZ-mScarlet* (Scale bar, 50 μm). mScarlet fluorescence is false-colored cyan. Average fluorescence across depth of a representative biofilm section is shown in the right-hand plot.

consistent with a model in which RpoS acts upstream of CbrAB, the first apparent step of the *P. aeruginosa* CCR pathway, to inhibit *phzM* translation and therefore methylated phenazine production. In other words, RpoS might inhibit CbrB-induced *crcZ* expression, leading to a larger pool of unsequestered Crc available to bind *phzM* transcript, and therefore lower levels of *phzM* translation in the WT when compared to Δ*rpoS*.

CCR-pathway Mutant Phentoypes Are Consistent with Roles of the Pathway in Regulating PhzM Translation and Carbon Source Utilization. Our observations linking RpoS to the CCR pathway and the inhibition of metabolic activity in biofilms suggest that RpoN, which is required for *crcZ* expression, could promote metabolic activity in biofilms. We addressed this by imaging thin sections of WT and Δ*rpoN* biofilms via SRS microscopy and found

that Δ*rpoN* biofilms showed lower levels of metabolic activity across depth than those formed by the WT (*SI Appendix*, Fig. S3). This observation is consistent with RpoN's role in the CCR pathway and the abrogation of methylated phenazine production in this mutant (47, 62). A second prediction that arises from the fact that RpoS inhibits *crcZ* expression (Fig. 3*D*) is that RpoS might hinder *P. aeruginosa*'s ability to transition to growth on nonpreferred carbon sources, as *crcZ* relieves Crc/Hfq repression of target mRNAs involved in the use of these substrates (63). To test this idea, we used a defined liquid growth medium with a highly preferred carbon source (i.e., succinate, on which *P. aeruginosa* shows low levels of *crcZ* expression) or with a nonpreferred carbon source (i.e., mannitol, which induces high levels of *crcZ* expression) (64). We found that the Δ*rpoS* mutant indeed showed a large increase in *crcZ* expression (*SI Appendix*, Fig. S4), and enhanced growth during the lag and exponential phases (*SI Appendix*, Fig. S5), during growth on mannitol when compared to WT. During growth on succinate, Δ*rpoS* did not show a large increase in *crcZ* expression or enhanced growth during the lag or exponential phases of growth. The Δ*rpoS* mutant did, however, show an increased growth yield relative to WT during growth on succinate, which may arise from independent effects of this mutation.

Due to its role in stabilizing Hfq's interaction with target transcripts such as that of *phzM*, mutants lacking Crc overproduce PhzM and methylated phenazines (47, 65) (Fig. 3*B*). Having observed that Δ*rpoS* and BigBlue—two mutants with elevated methylated phenazine production—show increased metabolic activity at depth in biofilms, we wondered whether this correlation would extend to the Δ*crc* mutant. We used SRS microscopy to image Δ*crc* and Δ*phz*Δ*crc* biofilm thin sections and found that the Δ*crc* mutant also showed increased metabolic activity across depth in a phenazine-dependent manner (Fig. 4*A*).

CCR-pathway Mutants Are Sensitive to Phenazines. The phenotypes we observed for the Δ*rpoS* (Fig. 1*B*) and Δ*crc* mutants indicate that RpoS and Hfq/Crc inhibit physiological processes–leading to decreased metabolic activity and growth–raising the question of whether RpoS and Hfq/Crc activity have any benefits for PA14 under the conditions used here. In other words, do RpoS and/or Hfq/Crc have positive impacts that outweigh their inhibition of metabolic activity and growth? Because previous work has shown that pyocyanin can be toxic to *P. aeruginosa* under specific conditions (33), we sought to test whether RpoS and/or Hfq/Crc may protect *P. aeruginosa* from potential negative effects of phenazines.

We took three approaches to testing whether RpoS and/or Hfq/Crc mitigate the toxicity of phenazines. First, we plated the WT and the Δ*crc* and Δ*rpoS* mutants on medium containing the synthetic compound phenazine methosulfate (PMS). PMS is structurally similar to the methylated phenazines produced by *P. aeruginosa* and we have shown that other mechanisms of *P. aeruginosa* self-protection are active against this compound (34, 35). We found that Δ*crc*, but not Δ*rpoS*, showed a greater inhibition of growth by PMS than the WT (Fig. 4*B*). The Δ*crc* phenotype is in line with previous work in *P. aeruginosa* strain PAO1, which indicated that the Δ*crc* mutation affects redox homeostasis, tolerance of oxidizing agents, and expression of genes involved in the oxidative stress response (66). In the absence of Crc, target mRNAs whose translation would be repressed by Hfq/Crc in the wild-type background are translated. Evidence suggests that these include proteins that carry out steps in the Entner-Doudoroff and

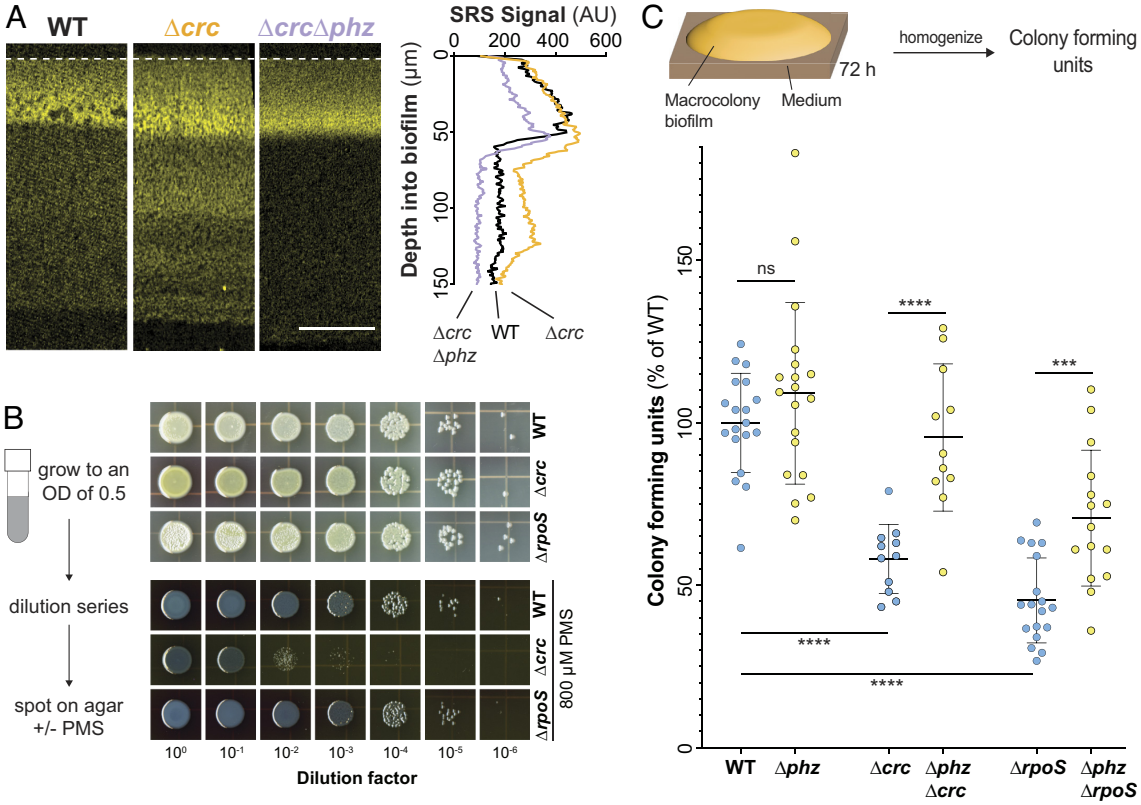

Fig. 4. Like *rpoS*, *crc* dampens phenazine-supported metabolic activity but contributes to phenazine resistance. (*A*) SRS images of thin sections prepared from WT, Δ*crc*, and Δ*crc*Δ*phz* biofilms. SRS signal is false-colored yellow and the average signal across depth is shown in the right-hand plot (Scale bar, 50 μm). (*B*) *Left*: Scheme depicting experimental design. Right: Growth of WT, Δ*rpoS*, and Δ*crc* on 1% tryptone, 1% agar medium without or with 800 μM PMS. For (*A*) and (*B*), experiments were performed with biological triplicates and representative data are shown. (*C*) *Top*: Scheme depicting experimental design. *Bottom*: Quantification of colony-forming units from 3-d-old biofilms, displayed as a percentage of the WT value. Each point represents a biological replicate. *P* values were calculated using unpaired, two-tailed *t* tests (***$P < 0.001$ and ****$P < 0.0001$).

pentose phosphate pathways and that their increased levels in Δ*crc* lead to effects on redox balancing. In the Δ*rpoS* background, RpoS-dependent effects on *crcZ* levels are absent but Crc is still present, and it is possible that other regulators modulate *crcZ* levels to allow Crc to contribute to oxidative stress resistance in the presence of PMS.

In our second approach, we grew WT and mutant biofilms under standard conditions before harvesting, homogenizing, and plating for colony-forming units (CFUs). We found that Δ*rpoS* and Δ*crc* biofilms contain ~50% fewer CFUs than their WT counterparts and that this effect is partially reversed in the phenazine-null background (Fig. 4*C*). In our third and final approach, we sought to identify which biofilm region may benefit most from RpoS and/or Crc activity. We incubated mature biofilms on medium containing propidium iodide (PI), a dye that shows increased staining in biofilm regions with low viability. We observed increased staining at the biofilm-air interface in Δ*rpoS* biofilms when compared to those formed by the WT (*SI Appendix*, Fig. S6). This result is in line with our observation that RpoS inhibits *crcZ* expression specifically in this zone. Taken together, our findings highlight the long-range effects of localized sigma factor activity and metabolite production on the metabolism and survival of physiologically differentiated subpopulations in biofilms.

Discussion

Besides *P. aeruginosa* (67), several other pseudomonad species including *P. chlororaphis* and *P. synxantha* make the phenazine PCA (38, 68, 69). However, among these species, *P. aeruginosa* is unusual in its ability to produce methylated phenazines (35). Out of the variety of *P. aeruginosa* phenazines, those that are methylated have the most dramatic effects on biofilm matrix production and morphogenesis (34), antibiotic tolerance (31, 70), and—as shown in this study—metabolic activity. In this context, it is interesting that, as indicated by our findings, phenazine methylation is linked to global regulatory pathways that respond to carbon source identity and abundance. Phenazine production itself is a carbon- and nitrogen-consuming process (71), but in addition, methylated phenazines—which have relatively high redox potentials and reactivities—in particular have the effect of oxidizing the cytoplasm and activating cellular defense mechanisms including the expression of efflux pumps (70, 72–74). Because nutritional conditions affect the cellular carbon/nitrogen balance and could serve as proxy signals for environments in which these mechanisms contribute to fitness, it could be beneficial for *P. aeruginosa* to control phenazine methylation so that it occurs when specific types of carbon sources are available (75).

Fig. 5 *A* and *B* depict models of the integrated effects of RpoS and the CCR pathway on metabolic activity and survival in PA14 biofilms. The two-component system CbrAB, which functions as the first step in the pseudomonad CCR pathway, is sensitive to carbon source identity but its precise activating signal has not been described. Several studies have suggested that the CbrA-activating signal is intracellular and representative of the carbon/nitrogen balance (52, 64, 76, 77). Once activated, CbrA transfers a phosphoryl group to CbrB, which binds directly to the *crcZ* promoter and recruits RpoN-containing RNA polymerase to stimulate transcription (52). The sRNA CrcZ binds and sequesters Crc/Hfq, allowing translation of *phzM* mRNA and thereby promoting phenazine methylation (47). In WT PA14 biofilms (Fig. 1) metabolic activity is supported by oxygen available at the biofilm-air interface and by methylated phenazine available at depth in the hypoxic/anoxic region. In Δ*rpoS* and Δ*crc* biofilms (Figs. 1*B* and 4*A*) metabolic activity is enhanced throughout the biofilm due to increased production of methylated phenazine. In the Δ*crc* and Δ*rpoS* backgrounds, this enhanced metabolic activity apparently comes at a cost as evidenced by increased sensitivity to phenazines (Fig. 4*B* and *C*). Experiments in liquid cultures have indicated that the methylated phenazine pyocyanin is toxic to producing cells that are starved for carbon (33). Indeed, the fact that we observe maximal metabolic activity at a depth of ~30 to 50 μm, rather than at the biofilm–air interface, hints at the presence of an electron donor/carbon source gradient emanating from the biofilm base. Crc has also been shown to prevent the accumulation of reactive oxygen species and the activation of oxidative stress pathways (66). This suggests a tradeoff may exist in biofilms between the self-preservation of oxic cells and the

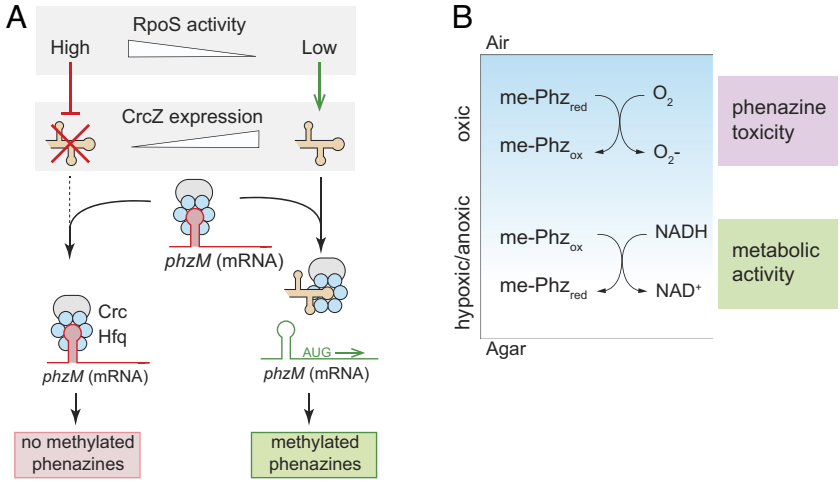

Fig. 5. RpoS affects pyocyanin production via the CCR pathway and is simultaneously beneficial for survival and detrimental for metabolic activity in distinct biofilm subzones. (*A*) Scheme depicting the regulatory relationship between RpoS activity and *phzM* translation. High RpoS activity indirectly inhibits production of the sRNA CrcZ, liberating the Crc/Hfq complex, which in turn represses *phzM* translation. When RpoS activity is low, *crcZ* is transcribed and the CrcZ sRNA binds to and sequesters the Crc/Hfq complex; this allows *phzM* translation to proceed. (*B*) Model depicting the differential effects of methylated phenazines in the oxic and hypoxic/anoxic subzones of a biofilm. We propose that methylated phenazines are toxic in the oxic subzone, due to low nutrient availability and the reactivity of phenazines with oxygen, and that cells in this region benefit from RpoS' activities, including its role in dampening phenazine methylation. Cells in the hypoxic/anoxic subzone, in contrast, benefit from phenazine methylation because methylated phenazine (specifically PYO) serves as an alternate acceptor of cellular reducing equivalents and support metabolic activity. NADH is shown as a representative carrier of cellular reducing equivalents. The blue shading represents the O_2 gradient.

potential metabolic activity of cells in hypoxic/anoxic regions of the biofilm, balanced by the dampening of phenazine methylation by RpoS acting via the CCR system.

We conclude that RpoS promotes expression of genes that enhance survival during carbon source limitation, but also inhibits expression of *crcZ*, at the biofilm–air interface. The mechanism of this inhibition is unclear but could arise from the effects of the RpoS regulon on *P. aeruginosa* metabolism; this regulon includes genes involved in primary metabolic pathways and RpoS activity could stimulate a shift in the *P. aeruginosa* metabolome that is sensed by CbrAB (18, 24). An alternative explanation could be that RpoS inhibits *crcZ* expression by competing with RpoN for binding to the RNA polymerase. However, previous analysis of sigma factor deletion strains does not show correlative positive associations between expression of RpoS-dependent genes in *rpoN*-deletion strains, nor vice versa (24), suggesting that this is not the mechanism of RpoS-dependent *crcZ* repression. Regardless, we have observed that phenazine methylation is limited by an RpoS-dependent inhibition of *crcZ* expression at the surface of *P. aeruginosa* biofilms. Because methylated phenazine contributes to metabolic activity in the hypoxic/anoxic biofilm subzone, RpoS' effects "trickle down" to this region. RpoS- and Crc-dependent inhibition of methylated phenazine production in biofilms may therefore represent a physiological tradeoff that limits toxicity at the biofilm-air interface at the expense of metabolic activity at depth.

Materials and Methods

Strains and Growth Conditions. All bacterial strains used in this study are listed in *SI Appendix*, Table S1. For routine liquid culture growth, single colonies of *P. aeruginosa* UCBPP-PA14 were used to inoculate lysogeny broth (LB) or 1% tryptone, as specified in the text, and shaken at 37 °C, 200 rpm. Precultures for biofilm experiments were grown in liquid LB for 12–16 h, then diluted 1:100, or 1:50 for ΔrpoN backgrounds, in 2 mL LB and grown for 2.5 h at 37 °C to an OD(500 nm) of 0.4–0.6. These liquid cultures were spotted onto 1% tryptone 1% agar plates and incubated at 25 °C. Biofilm morphology was determined as described previously (78) on morphology assay plates made of 1% tryptone and 1% agar and containing 20 μg/mL Congo red and 30 μg/mL Coomassie blue (79). Images of colonies were taken using a Keyence VHX-1000 digital microscope. All planktonic cultures and biofilms were incubated in the dark.

To compare the growth dynamics and activities of reporters for individual strains, experiments were carried out in 96-well plate, black-sided, clear-bottomed plates (Greiner Bio-One). Strains were pregrown in glass culture tubes in liquid LB for 12–16 h, and these precultures were used to inoculate 200 μL of media at a dilution of 1:100 in 96-well plates. Plates were set to incubate at 25 °C with continuous shaking on the medium setting in a Biotek Synergy H1 plate reader. The defined medium used to test individual carbon sources was MOPS minimal medium (50 mM 4 morpholinepropanesulfonic acid (pH 7.2), 43 mM NaCl, 93 mM NH_4Cl, 2.2 mM KH_2PO_4, 1 μg/mL $FeSO_4{\cdot}7H_2O$, and 1 mM $MgSO_4{\cdot}7H_2O$). Growth was assessed by taking OD readings at 500 nm and fluorescence readings at excitation and emission wavelengths of 569 nm and 599 nm, respectively, every 30 min for up to 40 h.

Fluorescent Reporter Strain Construction. All plasmids used in this study are listed in *SI Appendix*, Table S2. To create reporters of promoter activity for the *crcZ* and *crc* genes, the respective 161-bp and 500-bp promoter regions upstream of the start codon were amplified by PCR using primers (*SI Appendix*, Table S3) that added KpnI and XhoI (P*crc*) or SpeI and XhoI (P*crcZ*) digest sites to the 5′ and 3′ ends of the sequence. Purified PCR products were digested and ligated into the pLD3208 vector at the multiple cloning site, upstream of the *mScarlet* sequence. The resulting plasmids were transformed into *E. coli* strain UQ950 and verified by sequencing. They were then moved into *P. aeruginosa* wild-type or mutant strains, as indicated in *SI Appendix*, Table S1, using biparental conjugation with *E. coli* strain S17-1. Selection for recombinants was carried out as previously described (38).

Creation of Deletion Mutant Strains. All plasmids used in this study are listed in *SI Appendix*, Table S2. Deletion constructs were made and deletion strains were produced via homologous recombination as previously described (38). Briefly, ~1-kb genomic flanks on either side of the gene to be deleted were amplified via PCR (primers listed in *SI Appendix*, Table S3) and ligated into digested pMQ30 plasmid (80) using *Saccharomyces cerevisiae* InvSc1 gap-closing repair. Successful ligations were selected with SD-Ura plates, grown, and the plasmid purified by miniprep. The plasmid was transformed into an *E. coli* mating strain, BW29427, and mated into the recipient *P. aeruginosa* strain. Plasmid integration into *P. aeruginosa* resulted in merodiploids, which are resolved by outgrowth in LB. Strains that successfully lost the integrated plasmid via homologous recombination were selected by growth on sucrose. The final clones were confirmed by PCR with primers flanking the excision site.

Creation of PCN-overproducing Strain. *phzH* was amplified using primers LD4528 and LD4529, and the rrnB terminator was amplified from pAKN69 (81) using primers LD4530 and LD4077 such that the two fragments had ~20 bp overlapping sequence similarity. An overlap PCR was performed using primers LD528 and LD4077 and the two fragments (~75 ng each) as template. The resulting fragment (PhzH-coding region with a terminator) was restriction-digest cloned into pAKN69 using SphI and NheI restriction enzymes. Because the coding region of PhzH contains a SphI cut site, this step was completed by first digesting the insert with EcoRI and gel purified the two fragments. The fragment with the beginning of the gene was cut with SphI and the end fragment cut with NheI. Then a three-way ligation was performed to assemble the complete plasmid. The resulting plasmid was transformed into *E. coli* BW29427, verified by sequencing, and introduced into PA14 using biparental conjugation with *E. coli* BW29427. Single recombinants were selected on LB agar plates containing 100 μg/mL gentamicin.

Biofilm Thin Sectioning. Macrocolony preparation and sectioning was performed as previously described with minor modifications (82). Bacterial subcultures were spotted onto 45 mL/15 mL two-layer 1% tryptone 1% agar in 100 mm × 15 mm square plates and grown for 72 h. The biofilms were overlaid with 25 mL of 1% molten agar, solidified, excised into histocassettes, and fixed in 4% paraformaldehyde in PBS for 24 h. After fixing, the samples were washed in a series of ethanol/PBS solutions in which the ethanol concentration was gradually increased to 100%. The samples were then washed with histoclear and subsequently infiltrated with molten paraffin wax. The samples were then placed in paraffin wax in wax molds and solidified overnight. The wax blocks containing the biofilm samples were shaped and the middle of the biofilms sectioned into 10-μm sections. The sections were floated on water and placed onto precharged glass slides. The slides were dried for 48 h, then heat fixed on a 45 °C hot plate for 45 min. After the slides had cooled, they were rehydrated by washing with histoclear followed by a series of ethanol/PBS solutions in which the ethanol concentration was gradually decreased to 0%. Once rehydrated, mounting media and a coverslip were placed on the slide, and the samples were imaged.

Stimulated Raman Scattering Microscopy. Five microliters of a bacterial subculture was spotted onto 45 mL/15 mL two-layer 1% tryptone 1% agar plates and grown for 72 h; then, the top layer and biofilm were transferred to 2 mL 1% tryptone 1% agar 50% D_2O and incubated at 25 °C for 5 h. Where indicated, the plates also contained the specified concentration of commercially available phenazines (pyocyanin: Cayman Chemical Company 10009594, PCN: Apexmol 550-89-0). The biofilms were then thin-sectioned as described above. For SRS microscopy, an integrated laser source (picoEMERALD, Applied Physics & Electronics, Inc.) was used to produce both a Stokes beam (1,064 nm, 6 ps, intensity modulated at 8 MHz) and a tunable pump beam (720–990 nm, 5–6 ps) at an 80-MHz repetition rate. The spectral resolution of SRS is FWHM = 6–7 cm^{-1}. These two spatially and temporally overlapped beams with optimized near-IR throughput were coupled into an inverted multiphoton laser-scanning microscope (FV1200MPE, Olympus). Both beams were focused on the biofilm samples through a 25X water objective (XLPlan N, 1.05 N.A. MP, Olympus) and collected with a high N.A. oil condenser lens (1.4 N.A., Olympus) after the sample. By removing the Stokes beam with a high O.D. bandpass filter (890/220 CARS, Chroma Technology), the pump beam is detected with a large area Si photodiode (FDS1010, Thorlabs) reverse-biased by 64 DC voltage. The output current of the photodiode was electronically filtered (KR 2724, KR electronics), terminated with 50 Ω, and demodulated with a lock-in amplifier (HF2LI, Zurich Instruments) to achieve near shot-noise-limited

sensitivity. The stimulated Raman loss signal at each pixel was sent to the analog interface box (FV10-ANALOG, Olympus) of the microscope to generate the image. All images were acquired with 80 μs time constant at the lock-in amplifier and 100 μs pixel dwell time (~27 s per frame of 512 × 512 pixels). Measured after the objectives, 40 mW pump power and 120 mW Stokes beam were used to image the carbon-deuterium 2,183 cm^{-1} and off-resonance 2,004 cm^{-1} channels.

Image analysis was performed using Fiji. For better visualization, all SRS sections were brightened in Fiji to a maximum brightness value of 800. Quantifications reflect the unmodified signal.

Oxygen Profiling of Biofilms. A 25-μm-tip oxygen microsensor (Unisense OX-25) was used to measure oxygen concentrations along the depth of biofilms grown for 72 h at 25 °C. Two-point calibration was used to calibrate the oxygen microsensor. The first calibration point was atmospheric oxygen using a calibration chamber (Unisense CAL300) containing water continuously bubbled with air. The second calibration point was a "zero" point using an anoxic solution of 0.1 M sodium ascorbate 0.1 M NaOH. Oxygen measurements were taken throughout the depth of the biofilm using a measurement time of 3 s and a wait time between measurements of 3 s. The step size between measurements was 5 μm and controlled by a micromanipulator (Unisense MM33). Profiles were recorded using a multimeter (Unisense) and the SensorTrace Profiling software (Unisense).

Phenazine Detection by HPLC and Spectrophotometry. Ten μL of bacterial subculture was spotted onto 4 mL of 1% tryptone 1% agar in 30-mm circular petri plates and grown for 72 h at 25 °C. The biofilm and agar were placed into 5 mL of 100% methanol and nutated overnight at room temperature to extract the phenazines. To measure the amount of aeruginosins, 600 μL of the methanol extract was added to 600 μL of chloroform, briefly vortexed, and allowed to settle into fractions. After separation, 100 μL of the top aqueous fraction was put into a 96-well plate and read in a plate reader. To quantify aeruginosin levels, the samples were excited at 520 nm and the emission read at 620 nm. The results presented are all normalized relative to the signal of PA14 biofilms. To measure levels of PCA, PCN, and pyocyanin, the methanol extract was filtered through 0.22-μm cellulose acetate Spin-X centrifuge tube filters (Costar); then, 200 μL was transferred to HPLC vials for analysis on an Agilent 1100 HPLC system. A 50-μL sample was loaded on a Kinetex Biphenyl reverse phase column (Phenomenex 00F-4622-E0). HPLC-based separation was carried out using a gradient of water-0.02% formic acid (solvent A) to methanol-0.02% formic acid (solvent B) at a flow rate of 0.4 mL/min using the following protocol: linear gradient from 40% to 100% solvent B for 30 min followed by 5 min of 100% solvent B. The total method time was 35 min with a 5-min postwash of 100% solvent B. The resulting peaks at 366 nm were identified and quantified relative to samples of purified PCA, PCN, and pyocyanin run in known concentrations. The retention times for pyocyanin, PCN, and PCA are 9.5 min, 26 min, and 31.5 min, respectively.

PMS Sensitivity Assay. Precultures of strains of interest were grown for 16 h at 37 °C, 200 rpm, and then subcultured at a dilution of 30 μL into 3 mL LB medium in VWR 13 x 100 mm glass culture tubes. Subcultures were grown for about 2.5 h to an OD (500 nm) of approximately 0.55, then normalized to an OD (500 nm) of 0.5 before serial dilution. Five microliters of each dilution was spotted onto 10-cm square plates containing 60 mL of 1% tryptone 1% agar medium with or without 800 μM PMS (Fisher Scientific, ICN10095510). Biofilms were incubated for 48 h at 25 °C before scanning on an Epson Expression 11000XL photo scanner. The brightness of all images was adjusted in the same way to a value of 150 using Adobe Photoshop for ease of visualization.

Colony-Forming Unit Assay. Macrocolony biofilms were grown for 3 d on 1% tryptone 1% agar. Each biofilm was transferred to a 2-mL tube with a sealing O-ring (Benchmark Scientific D1031-T20) containing 1 mL of phosphate-buffered saline and 0.5 g of ceramic beads (Fisher Scientific 15-340-159). Samples were homogenized using an Omni Bead Ruptor 12 (Omni 19-050) on high for 90 s at 4 °C. Samples were left on ice for 10 min to allow bubbles to clear. Serial dilutions in PBS were performed until the countable dilution of 10^{-6}. Ten microliters were spotted on 1% tryptone 1.5% agar plates, which were tilted vertically to allow the spot to run down the plate and thereby increase the growth area. After 16 h of growth at 37 °C, single colonies were counted and recorded.

Propidium Iodide Staining. Five microliters of a bacterial subculture was spotted onto 45 mL/15 mL two-layer 1% tryptone 1% agar plates were grown for 72 h, then the top layer and biofilm was transferred to 30 mL of 1% tryptone 1% agar 50 μM propidium iodide (Sigma-Aldrich P4864-10ML) and incubated at 25 °C for 6 h. The biofilms were then thin-sectioned as described above and imaged on a ZEISS Axio Zoom.V16.

Data, Materials, and Software Availability. All study data are included in the article and/or *SI Appendix*.

ACKNOWLEDGMENTS. This work was supported by NIH/NIAID grant R01AI103369 to L.E.P.D. and NIH/NIBIB grant R01EB029523 to W.M.

Author affiliations: [a]Department of Biological Sciences, Columbia University, New York, NY 10027; and [b]Department of Chemistry, Columbia University, New York, NY 10027

1. C. R. Evans, C. P. Kempes, A. Price-Whelan, L. E. P. Dietrich, Metabolic heterogeneity and cross-feeding in bacterial multicellular systems. *Trends Microbiol.* **28**, 732–743 (2020).
2. J. Jo, A. Price-Whelan, L. E. P. Dietrich, Gradients and consequences of heterogeneity in biofilms. *Nat. Rev. Microbiol.* **20**, 593–607 (2022), https:/doi.org/10.1038/s41579-022-00692-2.
3. J. van Gestel, H. Vlamakis, R. Kolter, Division of labor in biofilms: The ecology of cell differentiation. *Microbiol Spectr* **3**, MB-0002-2014 (2015).
4. K. S. Williamson *et al.*, Heterogeneity in *Pseudomonas aeruginosa* biofilms includes expression of ribosome hibernation factors in the antibiotic-tolerant subpopulation and hypoxia-induced stress response in the metabolically active population. *J. Bacteriol.* **194**, 2062–2073 (2012).
5. P. S. Stewart, M. J. Franklin, Physiological heterogeneity in biofilms. *Nat. Rev. Microbiol.* **6**, 199–210 (2008).
6. Z.-F. Lim, P. C. Ma, Emerging insights of tumor heterogeneity and drug resistance mechanisms in lung cancer targeted therapy. *J. Hematol. Oncol.* **12**, 134 (2019).
7. K.-T. Chou *et al.*, A segmentation clock patterns cellular differentiation in a bacterial biofilm. *Cell* **185**, 145–157.e13 (2022).
8. A. Feklístov, B. D. Sharon, S. A. Darst, C. A. Gross, Bacterial sigma factors: A historical, structural, and genomic perspective. *Annu. Rev. Microbiol.* **68**, 357–376 (2014).
9. D. Missiakas, S. Raina, The extracytoplasmic function sigma factors: Role and regulation. *Mol. Microbiol.* **28**, 1059–1066 (1998).
10. G. Klauck, D. O. Serra, A. Possling, R. Hengge, Spatial organization of different sigma factor activities and c-di-GMP signalling within the three-dimensional landscape of a bacterial biofilm. *Open Biol.* **8**, 180066 (2018).
11. J. K. Knobloch *et al.*, Biofilm formation by *Staphylococcus epidermidis* depends on functional RsbU, an activator of the sigB operon: Differential activation mechanisms due to ethanol and salt stress. *J. Bacteriol.* **183**, 2624–2633 (2001).
12. C. W. Hall *et al.*, *Pseudomonas aeruginosa* biofilm antibiotic resistance gene ndvB expression requires the RpoS stationary-phase sigma factor. *Appl. Environ. Microbiol.* **84**, e02762-17 (2018).
13. A. Bazire *et al.*, The sigma factor AlgU plays a key role in formation of robust biofilms by nonmucoid *Pseudomonas aeruginosa*. *J. Bacteriol.* **192**, 3001–3010 (2010).
14. J. D. Helmann, Where to begin? Sigma factors and the selectivity of transcription initiation in bacteria. *Mol. Microbiol.* **112**, 335–347 (2019).
15. H. E. Schellhorn, Function, evolution, and composition of the RpoS regulon in *Escherichia coli*. *Front. Microbiol.* **11**, 560099 (2020).
16. F. Mika, R. Hengge, Small RNAs in the control of RpoS, CsgD, and biofilm architecture of *Escherichia coli*. *RNA Biol.* **11**, 494–507 (2014).
17. S. Gottesman, Trouble is coming: Signaling pathways that regulate general stress responses in bacteria. *J. Biol. Chem.* **294**, 11685–11700 (2019).
18. M. Schuster, A. C. Hawkins, C. S. Harwood, E. P. Greenberg, The *Pseudomonas aeruginosa* RpoS regulon and its relationship to quorum sensing. *Mol. Microbiol.* **51**, 973–985 (2004).
19. A. Rodríguez-Rojas, A. Oliver, J. Blázquez, Intrinsic and environmental mutagenesis drive diversification and persistence of *Pseudomonas aeruginosa* in chronic lung infections. *J. Infect. Dis.* **205**, 121–127 (2012).
20. M. D. Maciá *et al.*, Hypermutation is a key factor in development of multiple-antimicrobial resistance in *Pseudomonas aeruginosa* strains causing chronic lung infections. *Antimicrob. Agents Chemother.* **49**, 3382–3386 (2005).
21. O. Ciofu, B. Riis, T. Pressler, H. E. Poulsen, N. Høiby, Occurrence of hypermutable *Pseudomonas aeruginosa* in cystic fibrosis patients is associated with the oxidative stress caused by chronic lung inflammation. *Antimicrob. Agents Chemother.* **49**, 2276–2282 (2005).
22. A. Oliver, R. Cantón, P. Campo, F. Baquero, J. Blázquez, High frequency of hypermutable *Pseudomonas aeruginosa* in cystic fibrosis lung infection. *Science* **288**, 1251–1254 (2000).
23. E. Potvin, F. Sanschagrin, R. C. Levesque, Sigma factors in *Pseudomonas aeruginosa*. *FEMS Microbiol. Rev.* **32**, 38–55 (2008).
24. S. Schulz *et al.*, Elucidation of sigma factor-associated networks in *Pseudomonas aeruginosa* reveals a modular architecture with limited and function-specific crosstalk. *PLoS Pathog.* **11**, e1004744 (2015).
25. T. Wang *et al.*, An atlas of the binding specificities of transcription factors in *Pseudomonas aeruginosa* directs prediction of novel regulators in virulence. *eLife* **10**, e61885 (2021).
26. J. Jo, A. Price-Whelan, W. C. Cornell, L. E. P. Dietrich, Interdependency of respiratory metabolism and phenazine-associated physiology in *Pseudomonas aeruginosa* PA14. *J. Bacteriol.* **202**, e00700-19 (2020).
27. Y.-C. Lin *et al.*, Phenazines regulate nap-dependent denitrification in *Pseudomonas aeruginosa* biofilms. *J. Bacteriol.* **200**, e00031-18 (2018).

28. A. Ito, T. May, A. Taniuchi, K. Kawata, S. Okabe, Localized expression profiles of rpoS in *Escherichia coli* biofilms. *Biotechnol. Bioeng.* **103**, 975–983 (2009).
29. S. J. Suh *et al.*, Effect of rpoS mutation on the stress response and expression of virulence factors in *Pseudomonas aeruginosa*. *J. Bacteriol.* **181**, 3890–3897 (1999).
30. Y. Wang, S. E. Kern, D. K. Newman, Endogenous phenazine antibiotics promote anaerobic survival of *Pseudomonas aeruginosa* via extracellular electron transfer. *J. Bacteriol.* **192**, 365–369 (2010).
31. K. T. Schiessl *et al.*, Phenazine production promotes antibiotic tolerance and metabolic heterogeneity in *Pseudomonas aeruginosa* biofilms. *Nat. Commun.* **10**, 762 (2019).
32. S. H. Saunders *et al.*, Extracellular DNA promotes efficient extracellular electron transfer by pyocyanin in *Pseudomonas aeruginosa* biofilms. *Cell* **182**, 919–932.e19 (2020).
33. L. A. Meirelles, D. K. Newman, Both toxic and beneficial effects of pyocyanin contribute to the lifecycle of *Pseudomonas aeruginosa*. *Mol. Microbiol.* **110**, 995–1010 (2018).
34. H. Sakhtah *et al.*, The *Pseudomonas aeruginosa* efflux pump MexGHI-OpmD transports a natural phenazine that controls gene expression and biofilm development. *Proc. Natl. Acad. Sci. U.S.A.* **113**, E3538–E3547 (2016).
35. A. J. Sporer *et al.*, *Pseudomonas aeruginosa* PumA acts on an endogenous phenazine to promote self-resistance. *Microbiology* **164**, 790–800 (2018).
36. D. W. Basta, M. Bergkessel, D. K. Newman, Identification of fitness determinants during energy-limited growth arrest in *Pseudomonas aeruginosa*. *MBio* **8**, e01170-17 (2017).
37. K. D. Xu, M. J. Franklin, C. H. Park, G. A. McFeters, P. S. Stewart, Gene expression and protein levels of the stationary phase sigma factor, RpoS, in continuously-fed *Pseudomonas aeruginosa* biofilms. *FEMS Microbiol. Lett.* **199**, 67–71 (2001).
38. J. Jo, K. L. Cortez, W. C. Cornell, A. Price-Whelan, L. E. Dietrich, An orphan cbb3-type cytochrome oxidase subunit supports *Pseudomonas aeruginosa* biofilm growth and virulence. *eLife* **6**, e30205 (2017).
39. H. Dayton *et al.*, Cell arrangement impacts metabolic activity and antibiotic tolerance in *Pseudomonas aeruginosa* biofilms. bioRxiv [Preprint] (2023). https://doi.org/10.1101/2023.06.20.545666 (Accessed 28 August 2023).
40. F. Hu, L. Shi, W. Min, Biological imaging of chemical bonds by stimulated Raman scattering microscopy. *Nat. Methods* **16**, 830–842 (2019).
41. D. A. Recinos *et al.*, Redundant phenazine operons in *Pseudomonas aeruginosa* exhibit environment-dependent expression and differential roles in pathogenicity. *Proc. Natl. Acad. Sci. U.S.A.* **109**, 19420–19425 (2012).
42. D. V. Mavrodi *et al.*, Functional analysis of genes for biosynthesis of pyocyanin and phenazine-1-carboxamide from *Pseudomonas aeruginosa* PAO1. *J. Bacteriol.* **183**, 6454–6465 (2001).
43. E. A. Abu *et al.*, Cyclic voltammetric, fluorescence and biological analysis of purified aeruginosin A, a secreted red pigment of *Pseudomonas aeruginosa* PAO1. *Microbiology* **159**, 1736–1747 (2013).
44. G. S. Hansford, F. G. Holliman, R. B. Herbert, Pigments of *Pseudomonas* species. IV. In vitro and in vivo conversion of 5-methylphenazinium-1-carboxylate into aeruginosin A. *J. Chem. Soc. Perkin* **1**, 103–105 (1972).
45. K. Wang *et al.*, Overexpression of phzM contributes to much more production of pyocyanin converted from phenazine-1-carboxylic acid in the absence of RpoS in *Pseudomonas aeruginosa*. *Arch. Microbiol.* **202**, 1507–1515 (2020), https://doi.org/10.1007/s00203-020-01837-8.
46. L. E. P. Dietrich, T. K. Teal, A. Price-Whelan, D. K. Newman, Redox-active antibiotics control gene expression and community behavior in divergent bacteria. *Science* **321**, 1203–1206 (2008).
47. J. Huang, E. Sonnleitner, B. Ren, Y. Xu, D. Haas, Catabolite repression control of pyocyanin biosynthesis at an intersection of primary and secondary metabolism in *Pseudomonas aeruginosa*. *Appl. Environ. Microbiol.* **78**, 5016–5020 (2012).
48. E. Sonnleitner, U. Bläsi, Regulation of Hfq by the RNA CrcZ in *Pseudomonas aeruginosa* carbon catabolite repression. *PLoS Genet.* **10**, e1004440 (2014).
49. T. K. Kambara, K. M. Ramsey, S. L. Dove, Pervasive targeting of nascent transcripts by Hfq. *Cell Rep.* **23**, 1543–1552 (2018).
50. F. Corona, J. A. Reales-Calderón, C. Gil, J. L. Martínez, The development of a new parameter for tracking post-transcriptional regulation allows the detailed map of the *Pseudomonas aeruginosa* Crc regulon. *Sci. Rep.* **8**, 16793 (2018).
51. J. A. Wolff, C. H. MacGregor, R. C. Eisenberg, P. V. Phibbs Jr., Isolation and characterization of catabolite repression control mutants of *Pseudomonas aeruginosa* PAO. *J. Bacteriol.* **173**, 4700–4706 (1991).
52. E. Sonnleitner, L. Abdou, D. Haas, Small RNA as global regulator of carbon catabolite repression in *Pseudomonas aeruginosa*. *Proc. Natl. Acad. Sci. U.S.A.* **106**, 21866–21871 (2009).
53. W. Kong *et al.*, Dual GGDEF/EAL-domain protein RmcA controls the Type III secretion system of *Pseudomonas aeruginosa* by interaction with CbrB. *ACS Infect. Dis.* **8**, 2441–2450 (2022).
54. D. L. Mould, M. Stevanovic, A. Ashare, D. Schultz, D. A. Hogan, Metabolic basis for the evolution of a common pathogenic *Pseudomonas aeruginosa* variant. *eLife* **11**, e76555 (2022).
55. P. Pusic *et al.*, Cross-regulation by CrcZ RNA controls anoxic biofilm formation in *Pseudomonas aeruginosa*. *Sci. Rep.* **6**, 39621 (2016).
56. A. Farewell, K. Kvint, T. Nyström, Negative regulation by RpoS: A case of sigma factor competition. *Mol. Microbiol.* **29**, 1039–1051 (1998).
57. A. P. Lenz, K. S. Williamson, B. Pitts, P. S. Stewart, M. J. Franklin, Localized gene expression in *Pseudomonas aeruginosa* biofilms. *Appl. Environ. Microbiol.* **74**, 4463–4471 (2008).
58. P. S. Stewart *et al.*, Contribution of stress responses to antibiotic tolerance in *Pseudomonas aeruginosa* biofilms. *Antimicrob. Agents Chemother.* **59**, 3838–3847 (2015).
59. A. C. Pérez-Osorio, K. S. Williamson, M. J. Franklin, Heterogeneous rpoS and rhlR mRNA levels and 16S rRNA/rDNA (rRNA gene) ratios within *Pseudomonas aeruginosa* biofilms, sampled by laser capture microdissection. *J. Bacteriol.* **192**, 2991–3000 (2010).
60. D. L. Bellin *et al.*, Electrochemical camera chip for simultaneous imaging of multiple metabolites in biofilms. *Nat. Commun.* **7**, 10535 (2016).
61. L. Abdou, H.-T. Chou, D. Haas, C.-D. Lu, Promoter recognition and activation by the global response regulator CbrB in *Pseudomonas aeruginosa*. *J. Bacteriol.* **193**, 2784–2792 (2011).
62. Z. Cai *et al.*, RpoN regulates virulence factors of *Pseudomonas aeruginosa* via modulating the PqsR quorum sensing regulator. *Int. J. Mol. Sci.* **16**, 28311–28319 (2015).
63. K. Bharwad, S. Rajkumar, Rewiring the functional complexity between Crc, Hfq and sRNAs to regulate carbon catabolite repression in *Pseudomonas*. *World J. Microbiol. Biotechnol.* **35**, 140 (2019).
64. M. Valentini *et al.*, Hierarchical management of carbon sources is regulated similarly by the CbrA/B systems in *Pseudomonas aeruginosa* and *Pseudomonas putida*. *Microbiology* **160**, 2243–2252 (2014).
65. X. Y. Pei *et al.*, Architectural principles for Hfq/Crc-mediated regulation of gene expression. *eLife* **8**, e43158 (2019).
66. F. Corona, J. L. Martínez, P. I. Nikel, The global regulator Crc orchestrates the metabolic robustness underlying oxidative stress resistance in *Pseudomonas aeruginosa*. *Environ. Microbiol.* **21**, 898–912 (2019).
67. B. Valot *et al.*, What it takes to be a *Pseudomonas aeruginosa*? The core genome of the opportunistic pathogen updated. *PLoS ONE* **10**, e0126468 (2015).
68. A. Biessy, M. Filion, Phenazines in plant-beneficial *Pseudomonas* spp.: Biosynthesis, regulation, function and genomics. *Environ. Microbiol.* **20**, 3905–3917 (2018).
69. D. Garrido-Sanz *et al.*, Classification of isolates from the *Pseudomonas fluorescens* complex into phylogenomic groups based in group-specific markers. *Front. Microbiol.* **8**, 413 (2017).
70. L. A. Meirelles, E. K. Perry, M. Bergkessel, D. K. Newman, Bacterial defenses against a natural antibiotic promote collateral resilience to clinical antibiotics. *PLoS Biol.* **19**, e3001093 (2021).
71. W. Blankenfeldt, J. F. Parsons, The structural biology of phenazine biosynthesis. *Curr. Opin. Struct. Biol.* **29**, 26–33 (2014).
72. L. E. P. Dietrich, A. Price-Whelan, A. Petersen, M. Whiteley, D. K. Newman, The phenazine pyocyanin is a terminal signalling factor in the quorum sensing network of *Pseudomonas aeruginosa*. *Mol. Microbiol.* **61**, 1308–1321 (2006).
73. Lars E. Dietrich *et al.*, Bacterial community morphogenesis is intimately linked to the intracellular redox state. *J. Bacteriol.* **195**, 1371–1380 (2013).
74. M. Rozner *et al.*, Rewiring of gene expression in *Pseudomonas aeruginosa* during diauxic growth reveals an indirect regulation of the MexGHI-OpmD efflux pump by Hfq. *Front. Microbiol.* **13**, 919539 (2022).
75. J. L. Martínez, F. Rojo, Metabolic regulation of antibiotic resistance. *FEMS Microbiol. Rev.* **35**, 768–789 (2011).
76. T. Nishijyo, D. Haas, Y. Itoh, The CbrA-CbrB two-component regulatory system controls the utilization of multiple carbon and nitrogen sources in *Pseudomonas aeruginosa*. *Mol. Microbiol.* **40**, 917–931 (2001).
77. E. Monteagudo-Cascales, E. Santero, I. Canosa, The regulatory hierarchy following signal integration by the CbrAB two-component system: Diversity of responses and functions. *Genes* **13**, 375 (2022).
78. C. Okegbe *et al.*, Electron-shuttling antibiotics structure bacterial communities by modulating cellular levels of c-di-GMP. *Proc. Natl. Acad. Sci. U.S.A.* **114**, E5236–E5245 (2017), https://doi.org/10.1073/pnas.1700264114.
79. L. Friedman, R. Kolter, Genes involved in matrix formation in *Pseudomonas aeruginosa* PA14 biofilms. *Mol. Microbiol.* **51**, 675–690 (2004).
80. R. M. Q. Shanks, N. C. Caiazza, S. M. Hinsa, C. M. Toutain, G. A. O'Toole, Saccharomyces cerevisiae-based molecular tool kit for manipulation of genes from Gram-negative bacteria. *Appl. Environ. Microbiol.* **72**, 5027–5036 (2006).
81. L. Lambertsen, C. Sternberg, S. Molin, Mini-Tn7 transposons for site-specific tagging of bacteria with fluorescent proteins. *Environ. Microbiol.* **6**, 726–732 (2004).
82. W. C. Cornell *et al.*, Paraffin embedding and thin sectioning of microbial colony biofilms for microscopic analysis. *J. Vis. Exp.* **113**, 57196 (2018), https://doi.org/10.3791/57196.